

LETTER

Mechanism of actions of Oncocin, a proline-rich antimicrobial peptide, in early elongation revealed by single-molecule FRET

Dear Editor,

Proline-rich antimicrobial peptides (PrAMPs) are a class of antimicrobial peptides containing a high content of proline residues. PrAMPs selectively target Gram-negative bacteria through special transporters such as SmbA to enter cytoplasm (Mattiuzzo et al., 2007). On the other hand, PrAMPs present a low toxicity to mammalian cells, because they cannot effectively penetrate the mammalian cellular membrane (Hansen et al., 2012) or they are internalized through an endocytotic process to minimize interaction with cytosolic ribosomes (Tomasinsig et al., 2006). Therefore, PrAMPs are promising candidates to treat infections and to deliver drugs (Schmidt et al., 2016).

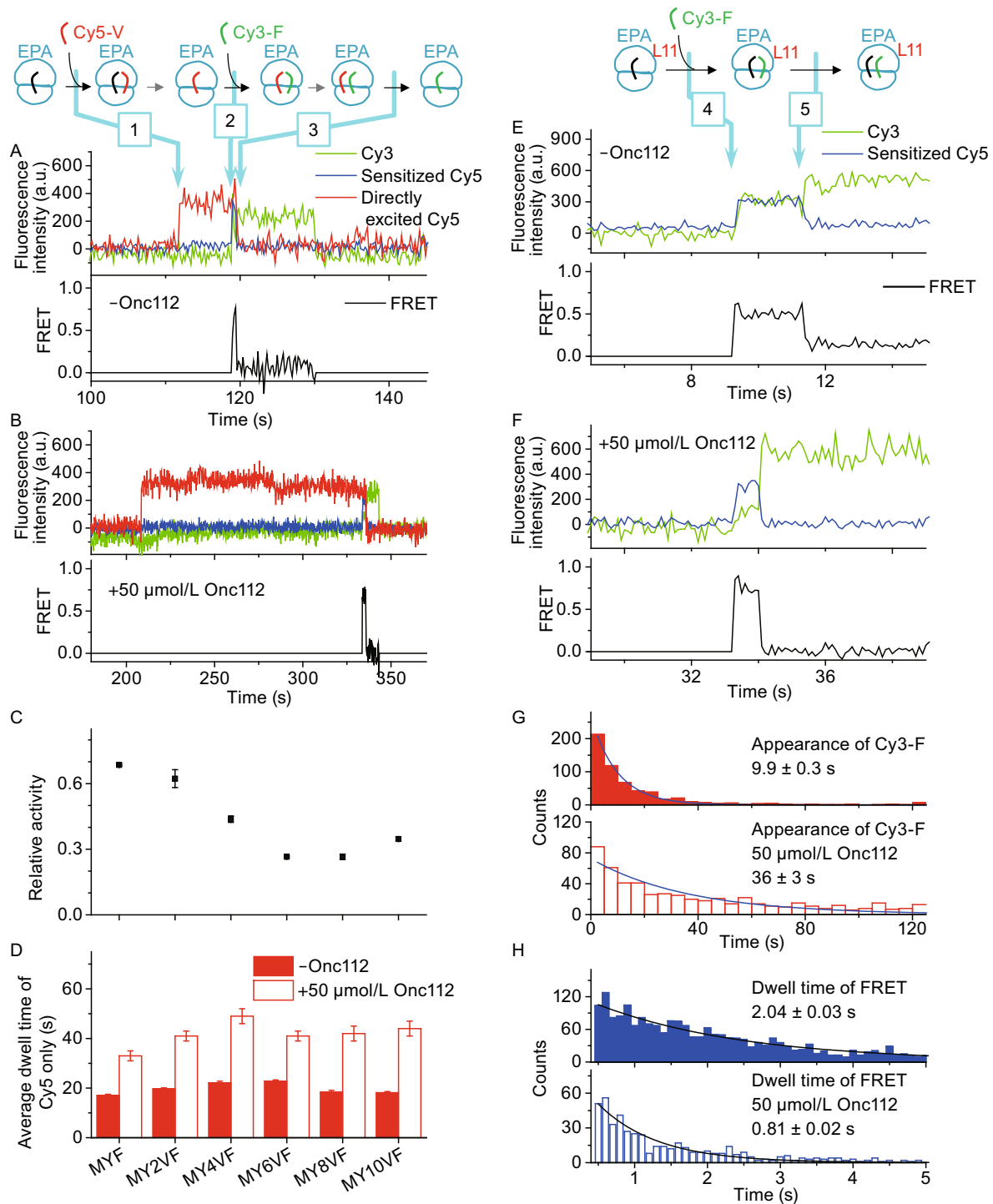
Oncocin represents a class of PrAMPs analogues modified from the *Oncopeltus* antibacterial peptides originally isolated from *Oncopeltus fasciatus* (milkweed bug). Oncocin has high antibacterial activity as its minimal inhibitory concentration (MIC) is around 1 $\mu\text{g}/\text{mL}$ (Knappe et al., 2010). Hoffmann group discovered that Onc112 can strongly bind to the ribosome with nanomolar dissociation constants (Knappe et al., 2011). Structures of Onc112 bound ribosomes illustrated that Onc112 occupies three adjacent functional sites, including the upper ribosomal exit tunnel, peptidyl transferase center (PTC), and ribosomal aminoacyl-tRNA (aa-tRNA) binding site (A-site) (Roy et al., 2015; Seefeldt et al., 2015), which suggests that Onc112 could hinder entrance of aa-tRNA into the ribosome. Structures of Onc112 bound ribosomes provide foundation to thoroughly elucidate its antibacterial mechanisms. Here, we apply single-molecule fluorescence resonance energy transfer (smFRET) assays we have developed (Peng et al., 2017) to characterize how Onc112 affects translation in several early elongation cycles.

Firstly, we characterized how Onc112 affects percentage of active ribosomes and elongation rates via smFRET between two adjacent tRNAs. Six different messenger RNAs (mRNAs) were used (Table S1). They all encode a common VF motif, which was placed at the 0, 2, 4, 6, 8, or 10 codon positions after the AUG start codon. Each active ribosome translating through the common VF motif produced one smFRET event as shown in Fig. 1A and 1B. The number of

Cy5-V/Cy3-F FRET events captured in the presence of Onc112, normalized by the number of FRET events in the absence of Onc112, was used to define the percentage of active ribosomes translating through the Phe codon (Fig. 1C). We found that, with Onc112, percentage of active ribosomes gradually decreases from ~70% in the second elongation cycle to ~30% in the eighth cycle. The Cy5-only state, shown between arrows 1 and 2 in Fig. 1A, corresponds to a full elongation cycle. Its dwell times were almost doubled in the presence of Onc112 (Figs. 1B, 1D, and S1), which clearly demonstrated that Onc112 slows overall elongation rate. In addition, Onc112 significantly hindered elongation at 1 $\mu\text{mol}/\text{L}$ or higher concentration (Fig. S2), which agrees with that its MIC is around 2 $\mu\text{mol}/\text{L}$ against *E. coli* (Knappe et al., 2011). In all, Onc112 slows overall elongation rates and reduces percentage of active ribosomes in early elongation cycles.

We examined how deletions in Onc112 affect its ability to inhibit elongation (Fig. S3). Onc ΔNr , a C-terminally truncated derivative, affected elongation in a similar manner as Onc112. However, Onc ΔVD , an N-terminally truncated derivative, caused minor inhibition. Our results agreed with previous findings that the N-terminus of Onc112 plays a key role in binding and deactivating the ribosome and its C-terminus mainly functions in cellular uptake (Seefeldt et al., 2015). Three control peptides, which were made of randomized or truncated Onc112 sequence, showed almost no inhibition on elongation (Fig. S4).

Next, we examined how rates of aa-tRNA delivery and translocation are effected by Onc112 via smFRET between ribosomal protein L11 and aa-tRNA. We mainly focused on the second elongation cycle of ribosomes programmed with mRNA MVF. Consistent with our previous findings, a high L11-tRNA FRET state (energy transfer efficiency $E = 0.4\text{--}0.8$) appeared when Cy3-F was delivered into the A-site (arrow 4 in Fig. 1E). After several seconds, L11-tRNA FRET decreased significantly ($E = 0.1\text{--}0.2$) when Cy3-F was translocated to the P-site (arrow 5 in Fig. 1E). The rate of aa-tRNA delivery in the second elongation cycle of ribosomes programmed with MVF, calculated from the delay time between injection of Cy3-F (defined as $t = 0$) and the



appearance of steady Cy3 and FRET intensities (arrow 4 in Fig. 1E), markedly decreased from $12.6 \pm 0.4 \text{ s}^{-1}(\mu\text{mol/L})^{-1}$ to $3.5 \pm 0.3 \text{ s}^{-1}(\mu\text{mol/L})^{-1}$ in the presence of Onc112 (Fig. 1G). Onc112 also decreased delivery rates of aa-tRNA in the first elongation cycle (Fig. S5). Our findings agreed with previous speculation derived from structural studies, which proposed that Onc112 could hinder entrance of aa-tRNA into the ribosome (Roy et al., 2015; Seefeldt et al.,

2015). On the other hand, translocation rate in the second elongation cycle of ribosomes programmed with MVF, calculated from dwell time of high L11-tRNA FRET state (Fig. 1E between arrows 4 and 5), increased from $0.49 \pm 0.01 \text{ s}^{-1}$ to $1.23 \pm 0.03 \text{ s}^{-1}$ in the presence of Onc112 (Fig. 1F and 1H). We found that conformational dynamics of ribosomal PRE-translocation (PRE) complexes prior to translocation were also affected by Onc112. 50 $\mu\text{mol/L}$

◀ **Figure 1. smFRET reveals that Onc112 inhibits elongation.**

(A and B) Typical real-time elongation traces measured using Cy5-V and Cy3-F without (A) or with (B) 50 $\mu\text{mol/L}$ Onc112, for ribosomes programmed with mRNAs containing a common VF motif (Table S1). Cy5-V, Cy3-F, and other necessary components were flowed onto microscope slides at time $t = 0$. In addition to Cy3 fluorescence (green) and sensitized emission of Cy5 (FRET, blue) under 532 nm laser excitation, Cy5 fluorescence (red) was collected under alternating 640 nm laser excitation. No fluorescence signal was detected until accommodation of Cy5-V (arrow 1). The Cy5-only state lasted for a full elongation cycle until accommodation of Cy3-F, the next aa-tRNA (arrow 2). When both Cy5-V and Cy3-F were present on the ribosome, fluorescence intensities of Cy3, sensitized Cy5 due to FRET from Cy3, and Cy5 directly excited by 640 nm laser were all detected (between arrows 2 and 3). Cy5 and FRET signals disappeared when Cy5-V dissociated from the E-site (arrow 3). (C) Relative activity of ribosomes elongated to the VF motif, defined by the number of Cy5-V/Cy3-F FRET events captured in the presence of Onc112 normalized by the number of FRET events captured in the absence of Onc112. (D) Average dwell times of the Cy5-only state in the absence and presence of Onc112 for six different mRNAs, which were calculated by exponential fitting of dwell time distributions shown in Fig. S1. (E and F) Typical real-time elongation traces of ribosomes programmed with mRNA MVF measured using Cy5-L11 and Cy3-F without (E) or with (F) 50 $\mu\text{mol/L}$ Onc112. Cy3-F and other necessary components were flowed onto microscope slides at time $t = 0$. Only Cy3 fluorescence (green) and sensitized emission of Cy5 (FRET, blue) were collected under 532 nm laser excitation. Formation of PRE-translocation complexes after Cy3-F accommodation led to appearance of Cy3 signal and high FRET efficiency between Cy5-L11 and Cy3-F (arrow 4). Translocation of Cy3-F from the A-site to P-site increased distance between Cy5-L11 and Cy3-F which caused decrease of FRET (arrow 5). (G and H) Dwell time distributions of POST-translocation (G, measured from $t = 0$ to arrow 4) and PRE-translocation complexes (H, measured between arrows 4 and 5) without Onc112 (solid bars) or with Onc112 (hollow bars). Time constants calculated by exponential fitting of dwell time distributions were listed with S.E. of fitting results. Number of events included are 599 (top) and 635 (bottom) in (G) and 2,536 (top) and 552 (bottom) in (H).

Onc112 destabilized the classical PRE state by decreasing its dwell time from 0.19 ± 0.01 s to 0.14 ± 0.01 s and stabilized the hybrid PRE states by increasing its dwell time from 0.20 ± 0.01 s to 0.26 ± 0.02 s, which would facilitate the following translocation step as shown by previous smFRET studies. The apparent rates of aa-tRNA delivery and translocation captured here, in the absence of Onc112, were close to our previous reported values and fit well within the range of $3.5\text{--}30$ $\text{s}^{-1}(\mu\text{mol/L})^{-1}$ (Pape et al., 1998; Johansson et al., 2008) and $0.4\text{--}2$ s^{-1} (Pan et al., 2007), respectively, reported by other groups. In summary, we

concluded that Onc112 mainly impairs delivery of aa-tRNA to the ribosome.

Aa-tRNAs are delivered to and selected by the ribosome via a multi-step process (Rodnina and Wintermeyer, 2001), which can be dissected using smFRET between P-site tRNA and incoming aa-tRNA at high data collecting rate (Geggier et al., 2010). We used a similar method to examine how Onc112 impairs delivery of aa-tRNA in details (Fig. 2A and 2B). Duration of FRET events clearly exhibited two components whose lifetimes were about ten-fold difference from each other (Fig. 2C and Table S2). In the absence of Onc112, the majority of FRET traces belonged to the long-lived component, which evolved from a transient low FRET state ($E = 0.2$) to a steady high FRET state ($E = 0.5\text{--}0.6$) until fluorescence signals disappeared due to photo-bleaching (Fig. 2A and 2C–F top panel). Onc112 significantly increased the proportion of the short-lived component, which evolved from a transient medium FRET state ($E = 0.4$) to another transient high FRET state ($E = 0.6$) (Fig. 2B and 2C–F middle panel). For these short-lived events, disappearance of FRET was caused by dissociation of Cy3-F from the ribosome because its disappearance rate was an order of magnitude faster than photo-bleaching rate. When we performed the same FRET measurements using ribosomes programmed with mRNA MVL (Table S1) which contained a CUC trinucleotide sequence, a near-cognate codon for Phe-tRNA^{Phe}, in the A-site, the majority of FRET traces belonged to the short-lived component (Fig. 2C–F bottom panel). At the same experimental conditions and instrumental configuration, no FRET event was captured when ribosomes contained non-cognate codons in the A-site. Together, these results indicated that the short-lived FRET events captured here represent aa-tRNA rejection events, which are likely to happen during the proofreading step of tRNA selection (Rodnina and Wintermeyer, 2001; Geggier et al., 2010). Onc112 significantly hinders aa-tRNA delivery by increasing rejection rate of the correct cognate aa-tRNA. About half of cognate aa-tRNA binding events are mistakenly rejected by the ribosome, which leads to slower overall aa-tRNA delivery rate in the presence of Onc112. Using mRNA MY6VF, we found similar behaviors that Onc112 increased rejection rate of cognate aa-tRNA at the eighth elongation cycle (Table S3).

When nascent peptide chain is elongated, Onc112 would have to move towards the exit of the ribosomal polypeptide exit tunnel to avoid physically clash with nascent peptide chain (Roy et al., 2015; Seefeldt et al., 2015). We performed a molecular dynamics (MD) simulation to estimate non-bonded interaction energy between Onc112 and the polypeptide exit tunnel when it moves towards the exit (Fig. S6). Our simulation indicated that previous structures (Roy et al., 2015; Seefeldt et al., 2015) captured the most stable binding site of Onc112, which gives the lowest interaction energy in our MD simulation. When Onc112 moves towards the exit site from its most stable site, interaction energy gradually increases until it reaches a plateau at ~ 15

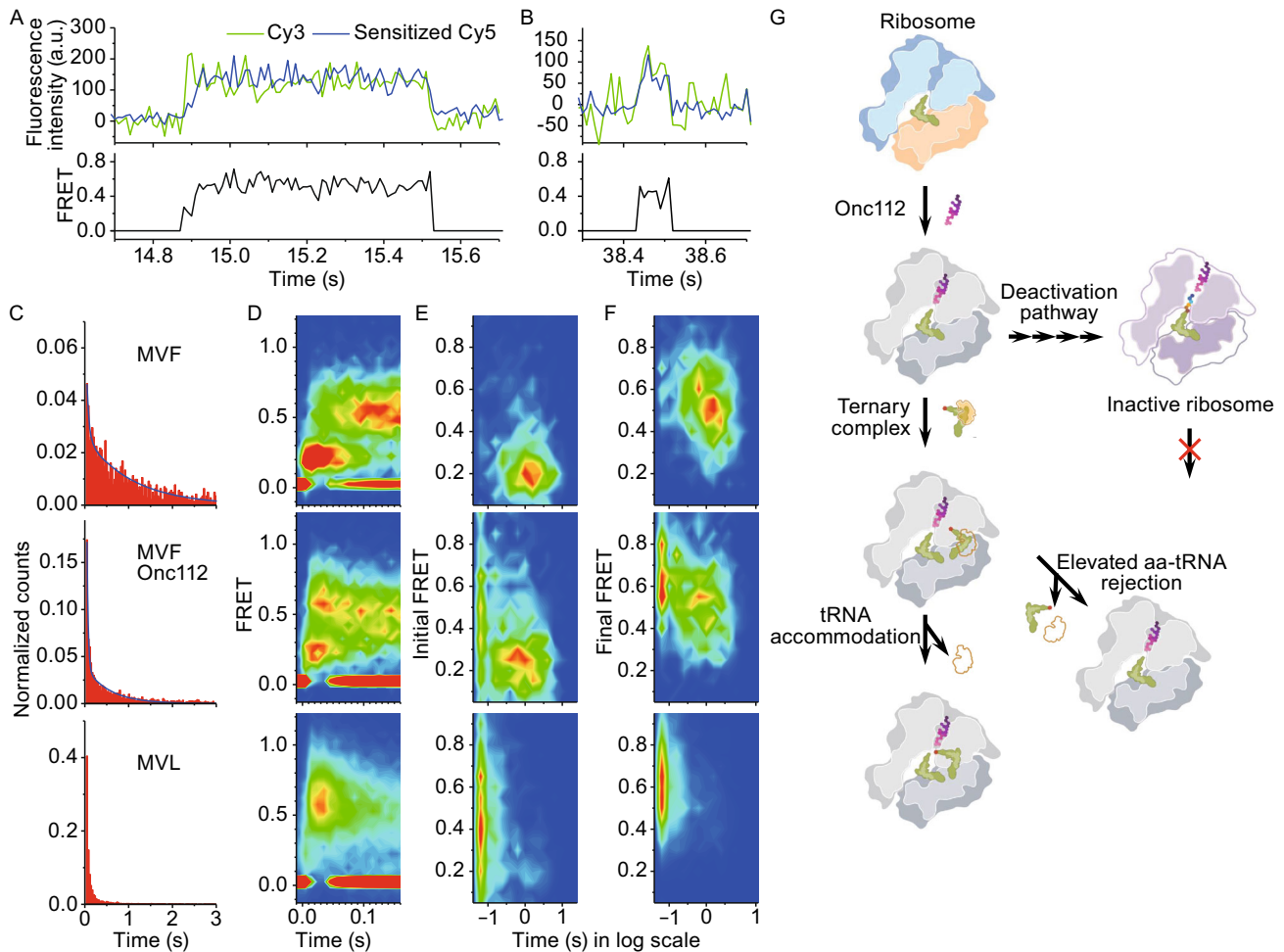


Figure 2. Onc112 inhibits aa-tRNA delivery and its proposed mechanisms. (A and B) Two types of typical real-time traces recorded while injecting 8 nmol/L Cy3-F ternary complex into flow channel, defined as time $t = 0$, containing immobilized ribosomal POST-translocation complexes with Cy5-V in the P-site. Both long (A) and short (B) FRET events were captured using ribosomes programmed with mRNAs MVF or MVL, whose A-sites contain cognate or near-cognate codons for Cy3-F, respectively. Only Cy3 fluorescence (green) and sensitized emission of Cy5 (FRET, blue) were collected under 532 nm laser excitation. (C) Dwell time distributions of all FRET events captured using mRNA MVF without (top panel) or with (middle panel) Onc112, or mRNA MVL without Onc112 (bottom panel). Details of fitting results were listed in Table S2. The same layout applies in (D–F). (D) FRET probability density plots as a function of time. All traces are aligned to the beginning of FRET events as $t = 0$, when both Cy3 and FRET signals appear simultaneously. (E and F) Heat maps constructed from initial FRET value when FRET events appear (E) or final FRET value right before FRET events disappear (F) vs. dwell times of FRET events. Each single-molecule event contributed as a single point in two-dimensional plots of FRET values vs. time. Heat maps were two-dimensional histograms made from all data points. Please notice that the top and bottom panels both contain one dominate population, whereas the middle panel has two populations. Number of events used here were listed in Table S2. (G) Proposed scheme to elucidate mechanisms of Onc112 in early elongation cycles. Two aspects have been highlighted. 1) Onc112 increases cognate aa-tRNA rejection rates, which leads to slower elongation rates. 2) Onc112 gradually deactivates 70% of ribosomes within 7–8 elongation cycles.

Å displacement (6–7 residues). Therefore, Onc112 causes extra energy cost to extend nascent peptide in the first 6–7 elongation cycles, which correlates with the gradual decrease of the percentage of active ribosomes in the first 8 cycles captured by smFRET (Fig. 1C). Once the nascent peptide is longer than 8 residues (>19 Å in Fig. S6), there is no extra energy cost to further move Onc112 towards the exit

and the percentage of active ribosomes remains almost constant (Fig. 1C).

Previous structural and biochemical studies suggested that Onc112 mainly acts in the elongation phase of protein synthesis (Roy et al., 2015; Seefeldt et al., 2015). Consistent with previous model, we found that Onc112 only moderately inhibits the formation of initiation complexes (Fig. S7). We


proposed a reaction scheme to illustrate mechanisms of Onc112 in early elongation (Fig. 2G), in which Onc112 binds within the polypeptide exit tunnel and moves towards the exit when nascent peptide gets elongated. We have revealed two major aspects. Firstly, Onc112 greatly accelerates rejection rate of cognate tRNA during aa-tRNA delivery. The percentage of rejected cognate tRNA is similar to the percentage of successfully accommodated tRNA, which implies that rate of rejection is elevated about an order of magnitude and is approximately the same as the rate of aa-tRNA accommodation (Rodnina and Wintermeyer, 2001). Elevated rejection rate of cognate tRNA leads to slow overall elongation rate, which would significantly hinder growth and survival of cells. Secondly, Onc112 gradually deactivates translating ribosomes in the early elongation cycles. About ~70% of ribosomes are active in the second elongation cycle, which further decrease to ~30% in the eighth elongation cycle. Strong correlation between interaction energy landscape estimated from MD simulation (Fig. S6) and the percentage of active ribosomes measured from smFRET assays (Fig. 1C) supports our model, in which Onc112 serves as a peptide exit tunnel blocker. Interactions between Onc112 and the ribosome introduce extra energy cost in the first 6–7 elongation cycles, which reduce elongation rates and gradually deactivate ~70% of ribosomes. The model we proposed here could represent conserved mechanism of action used by many other PrAMPs (Gagnon et al., 2016), which also provides guide to design and optimize future antibiotic drugs.

FOOTNOTES

This project is supported by funds from the National Natural Science Foundation of China (Grant No. 31570754), Tsinghua-Peking Joint Center for Life Sciences and Beijing Advanced Innovation Center for Structural Biology to CC and Lab Innovation Funding from Lab and Instrument Department, Tsinghua University to WW. The authors declare that they have no conflict of interest. This article does not contain any studies with human or animal subjects performed by the any of the authors.

OPEN ACCESS

This article is distributed under the terms of the Creative Commons Attribution 4.0 International License (<http://creativecommons.org/licenses/by/4.0/>), which permits unrestricted use, distribution, and reproduction in any medium, provided you give appropriate credit to the original author(s) and the source, provide a link to the Creative Commons license, and indicate if changes were made.

Sijia Peng^{1,2,3}, Mengyi Yang^{1,2,3}, Rui Ning Sun^{1,3,4}, Yang Liu¹, Wenjuan Wang^{1,5}, Qiaoran Xi¹, Haipeng Gong^{1,3,4}, Chunlai Chen^{1,2,3} 

¹ School of Life Sciences, Tsinghua University, Beijing 100084, China

² Tsinghua-Peking Joint Center for Life Sciences, Tsinghua University, Beijing 100084, China

³ Beijing Advanced Innovation Center for Structural Biology, Tsinghua University, Beijing 100084, China

⁴ MOE Key Laboratory of Bioinformatics, Tsinghua University, Beijing 100084, China

⁵ Technology Center for Protein Sciences, Tsinghua University, Beijing 100084, China

✉ Correspondence: chunlai@mail.tsinghua.edu.cn (C. Chen)

REFERENCES

- Gagnon MG, Roy RN, Lomakin IB, Florin T, Mankin AS, Steitz TA (2016) Structures of proline-rich peptides bound to the ribosome reveal a common mechanism of protein synthesis inhibition. *Nucleic Acids Res* 44:2439–2450. <https://doi.org/10.1093/nar/gkw018>
- Geggier P, Dave R, Feldman MB, Terry DS, Altman RB, Munro JB, Blanchard SC (2010) Conformational sampling of aminoacyl-tRNA during selection on the bacterial ribosome. *J Mol Biol* 399:576–595. <https://doi.org/10.1016/j.jmb.2010.04.038>
- Hansen A, Schafer I, Knappe D, Seibel P, Hoffmann R (2012) Intracellular toxicity of proline-rich antimicrobial peptides shuttled into mammalian cells by the cell-penetrating peptide penetratin. *Antimicrobial agents and chemotherapy* 56:5194–5201. <https://doi.org/10.1128/AAC.00585-12>
- Johansson M, Bouakaz E, Lovmar M, Ehrenberg M (2008) The kinetics of ribosomal peptidyl transfer revisited. *Mol Cell* 30:589–598. <https://doi.org/10.1016/j.molcel.2008.04.010>
- Knappe D, Piantavigna S, Hansen A, Mechler A, Binas A, Nolte O, Martin LL, Hoffmann R (2010) Oncocin (VDKPPYLPRPRPR-RIYNR-NH2): a novel antibacterial peptide optimized against gram-negative human pathogens. *Journal of medicinal chemistry* 53:5240–5247. <https://doi.org/10.1021/jm100378b>
- Knappe D, Kabankov N, Hoffmann R (2011) Bactericidal oncocin derivatives with superior serum stabilities. *International journal of antimicrobial agents* 37:166–170. <https://doi.org/10.1016/j.ijantimicag.2010.10.028>
- Mattiuzzo M, Bandiera A, Gennaro R, Benincasa M, Pacor S, Antcheva N, Scocchi M (2007) Role of the Escherichia coli SbmA in the antimicrobial activity of proline-rich peptides. *Mol Microbiol* 66:151–163. <https://doi.org/10.1111/j.1365-2958.2007.05903.x>
- Pan DL, Kirillov SV, Cooperman BS (2007) Kinetically competent intermediates in the translocation step of protein synthesis. *Mol Cell* 25:519–529
- Pape T, Wintermeyer W, Rodnina MV (1998) Complete kinetic mechanism of elongation factor Tu-dependent binding of aminoacyl-tRNA to the A site of the E. coli ribosome. *Embo J* 17:7490–7497. <https://doi.org/10.1093/emboj/17.24.7490>
- Peng S, Sun R, Wang W, Chen C (2017) Single-Molecule Photoactivation FRET: A General and Easy-To-Implement Approach To Break the Concentration Barrier. *Angewandte Chemie* 56:6882–6885. <https://doi.org/10.1002/anie.201702731>
- Rodnina MV, Wintermeyer W (2001) Fidelity of aminoacyl-tRNA selection on the ribosome: kinetic and structural mechanisms. *Annu Rev Biochem* 70:415–435. <https://doi.org/10.1146/annurev.biochem.70.1.415>

- Roy RN, Lomakin IB, Gagnon MG, Steitz TA (2015) The mechanism of inhibition of protein synthesis by the proline-rich peptide oncocin. *Nat Struct Mol Biol* 22:466–469. <https://doi.org/10.1038/nsmb.3031>
- Schmidt R, Ostorhazi E, Wende E, Knappe D, Hoffmann R (2016) Pharmacokinetics and in vivo efficacy of optimized oncocin derivatives. *The Journal of antimicrobial chemotherapy* 71:1003–1011. <https://doi.org/10.1093/jac/dkv454>
- Seefeldt AC, Nguyen F, Antunes S, Perebaskine N, Graf M, Arenz S, Inampudi KK, Douat C, Guichard G, Wilson DN et al (2015) The proline-rich antimicrobial peptide Onc112 inhibits translation by blocking and destabilizing the initiation complex. *Nat Struct Mol Biol* 22:470–475. <https://doi.org/10.1038/nsmb.3034>
- Tomasinsig L, Skerlavaj B, Papo N, Giabbai B, Shai Y, Zanetti M (2006) Mechanistic and functional studies of the interaction of a proline-rich antimicrobial peptide with mammalian cells. *J Biol Chem* 281:383–391. <https://doi.org/10.1074/jbc.M510354200>

Electronic supplementary material The online version of this article (<https://doi.org/10.1007/s13238-017-0495-2>) contains supplementary material, which is available to authorized users.